Frequency Response of a Thermistor Temperature Probe in Air

P. L. FUEHRER, C. A. FRIEHE, AND D. K. EDWARDS

Department of Mechanical and Aerospace Engineering, University of California, Irvine, California

(Manuscript received 13 October 1992, in final form 29 July 1993)

ABSTRACT

An analytical study was conducted of the thermal frequency response of an atmospheric temperature probe consisting of a thermistor bead with two lead wires soldered to thin support posts. Such probes are used in aircraft temperature sensors and for surface-layer turbulence studies. The results show the effects of the lead wires on the frequency response (amplitude and phase) of the probe for two end conditions of the lead wires: 1) fixed temperature at the mean free-stream value, and 2) adiabatic. For the smallest commercially available thermistor bead of approximately 200-μm diameter and for 20-μm-diameter platinum lead-wire lengths of about 0.8 mm, the conduction to the supports was found to be minimal for both end conditions. It was determined, however, that the lead wires themselves act as heat transfer fins and actually improve the frequency response over that of an ideal isolated bead. Model calculations show that the inclusion of multiple lead wires (four and six) connected mechanically, but not electrically or thermally, to supports would further improve the response. The thermal analysis is also applied to small type-E thermocouple junctions made of 12.5-, 25-, and 50-μm-diameter wires, and the results show that the lead wires also improve the frequency response.

1. Introduction

Research aircraft having temperature probes with fast time response are required in atmospheric studies to measure the turbulent heat flux, temperature spectra, and finescale features such as thermal plumes and sharp inversions. Typically, in situ sensors with resistance wire, thermistor, or thermocouple elements are used in the probes. For aircraft use, the sensing element can be in a housing designed to protect the element from rain and also provide a reasonably high recovery factor.[1] Recently, Friehe and Khelif (1993) compared in situ atmospheric temperature data from a Rosemount[2] 102 platinum wire probe to that from an identical Rosemount housing with the wire replaced with a small thermistor bead. The thermistor bead probe appeared to show less of a second slow time constant than the platinum wire probe, in which the wire is wound around a mica support structure. Payne et al. (1994) have theoretically analyzed the Rosemount 102 probe wound-wire configuration and have shown that it does exhibit a two-time-constant response due, in part, to conduction to the mica wire support structure.

A thermistor bead is also connected to a support structure, which in the 102 probe modification by Friehe and Khelif was a hot-wire anemometer probe consisting of two stainless steel needles to which the wires supporting the thermistor bead were soldered. The purpose of this work is to model the heat transfer characteristics of that probe to determine if there are any effects of the wires and supports on the frequency response. [Lumley (1962) derived the frequency response for heated thermistor beads used as anemometers but did not consider unheated beads as temperature sensors.] Paranthoen et al. (1982) have shown, for example, that for resistance wire sensors the length-to-diameter ratio of the suspended wire must be very large [$O(1000)$] for support effects to be negligible. The results of the present work are also applicable to the use of any bead-type sensor, such as the small thermocouples used by Cheney and Businger (1990) for micrometeorological measurements over land and by Lawson (1991) and Lawson and Rodi (1992) in the development of an in-cloud aircraft fast-response temperature sensor.

For the present study, a small commercially available bead[3] of the type used by Friehe and Khelif was photographed in a scanning electron microscope to determine its shape and dimensions, as shown in Fig. 1. The bead is seen to be an ellipsoid of revolution, that is, an ellipse rotated about its major axis, that is along the axis of the support wires. The major axis of the bead is about 223 μm, and the minor axis is about 160 μm. The method of construction apparently has two parallel support wires about 20 μm apart in the thermistor ma-

[1] The recovery factor is the fraction of the free-stream kinetic energy that is isentropically recovered as thermal energy in the fluid at the stagnation point of the sensor.

[2] Rosemount Engineering Company, Eagan, Minnesota.

[3] Model BB05, Thermometrics, Co., Edison, New Jersey.

Corresponding author address: Dr. Carl A. Friehe, Department of Mechanical Engineering, University of California, Irvine, CA 92717.

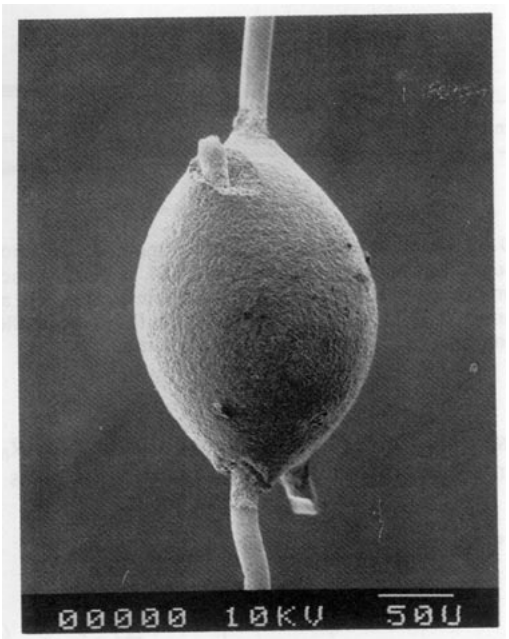

FIG. 1. Scanning electron microscope photograph of a typical thermistor bead (type BB05, Thermometrics, Edison, New Jersey). The horizontal bar is 50 μm. The platinum lead wires pass through the bead and protrude out the opposite side of the bead.

terial, and the two 20-μm-diameter platinum alloy lead wires pass through the entire body of the bead and are trimmed on opposite ends near the bead. The exact properties of the thermistor material and the alloy of the lead wires are not available, so approximate values were used for typical materials [see Sandborn (1972); Samsonov (1982); Thermometrics (1987)]. Also, for the model results shown, one airspeed (10 m s^{-1}) was chosen as representative of the restricted flow in the Rosemount 102 aircraft housing or for typical micrometeorological measurements. The resulting analyses are applicable to other speeds, provided the governing heat transfer relationships remain valid. The values for the properties of the thermistor bead, platinum lead wires, and atmospheric conditions are given in Table 1.

Figure 2 shows a sketch of the bead with lead wires mounted on a hot-wire anemometer probe.[4] The probe consists of two tapered stainless steel needles that are gold plated for soldering. The width between the needle ends is between 1.2 and 1.5 mm. The airflow is taken to be parallel to the needles and therefore perpendicular to the thermistor lead wires.

The analytical approach used here is to determine the thermal energy balance on the bead and supporting wire assembly and solve the resulting equation for the bead response in the time and frequency domain. Two limiting boundary conditions will be considered for the lead wires at the support posts: 1) the posts, and hence wire-end temperatures, are fixed at the mean free-stream temperature, and 2) the lead wires are insulated from the posts. The worst case (1) corresponds to the posts having so much thermal inertia that their temperatures do not respond to the fluctuations in the free stream, and therefore, the wire-end temperature remains fixed at the mean free-stream temperature. The best possible case (2) corresponds to no conduction to the posts; that is, the end temperature of the wire "floats." The actual situation lies somewhere between these two cases. If it can be shown that the transfer functions do not vary significantly between these two cases, then there is no need to model the heat transfer to and the conduction in the posts in detail.

2. Theory

a. Lumped-capacity analysis: Thermistor bead without supporting wires

The simplest model for the response of the thermistor bead neglects the conduction to or from the supporting wires and also models the bead as a "lumped capacitance" having negligible temperature gradients within the bead. The bead is modeled as a sphere with the same volume as the ellipsoid for the thermal mass and internal conduction and is modeled as a sphere with the same area as the ellipsoid for the heat transfer from the air. The assumption of an isothermal bead is valid for time scales significantly greater than the internal conduction time constant of the bead or, equivalently, for frequencies significantly lower than the multiplicative inverse of the internal conduction time constant. The internal conduction time constant for the bead τ_b is given as

$$\tau_b = \frac{r_{b,v}^2}{\alpha_b}, \tag{2.1}$$

where $r_{b,v}$ is the equivalent sphere radius for the same volume and α_b is the thermal diffusivity of the bead material. The thermal diffusivity is defined by

$$\alpha_b = \frac{k_b}{\rho_b c_b}, \tag{2.2}$$

where k_b is the bead thermal conductivity, ρ_b is the bead mass density, and c_b is the bead specific heat.

A thermal energy balance on the bead equates the time rate of change of internal energy of the bead to the energy flow at the surface (where incoming energy is taken as positive) plus the internal heat generation. Radiative transfer is neglected because the radiative heat transfer coefficient is about 0.5% of the convective heat transfer coefficient. The resulting energy equation is

$$\rho_b c_b V_b \frac{dT_b}{dt} = -h_b A_b (T_b - T_\infty) + I^2 R_b, \tag{2.3}$$

[4] Model 1210, TSI, Inc., St. Paul, Minnesota.

where V_b is the bead volume, T_b is the bead temperature, t is time, h_b is the bead surface-averaged heat transfer coefficient, A_b is the bead surface area, T_∞ is the air free-stream temperature, I is the sensing current flowing through the bead, and R_b is the electric resistance.

The electric resistance R_b is a function of temperature and is given by

$$R_b = R_{b,0} + \beta_b(T_b - T_0), \tag{2.4}$$

where

$$\beta_b = \left.\frac{dR_b}{dT}\right|_{T=T_0}. \tag{2.5}$$

For the solution of the time-varying temperature, the free-stream temperature is taken to be the sum of a mean part, T_0, plus a fluctuating part of amplitude ΔT_∞ and frequency ω; that is,

$$T_\infty = T_0 + \Delta T_\infty e^{i\omega t}. \tag{2.6}$$

(Radian frequency ω is used in the derivations; cyclic frequency $f = \omega/2\pi$ is used in the plots of the resulting solutions.)

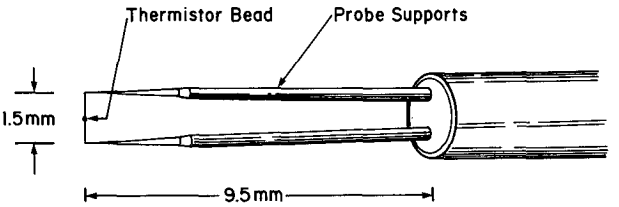

FIG. 2. Sketch of a thermistor bead as mounted on a hot-wire anemometer probe support (Model 1210, TSI, St. Paul, Minnesota). The probe support needles are gold-plated stainless steel. The airflow is assumed to be toward the probe body, parallel to the needles and perpendicular to the thermistor bead lead wires.

Using m_b for the bead mass, substituting for R_b and T_∞ in the energy equation and rearranging gives

$$\frac{dT_b}{dt} = -\frac{h_b A_b - I^2\beta_b}{m_b c_b}(T_b - T_0) + \frac{I^2 R_{b,0}}{m_b c_b} + \frac{h_b A_b}{m_b c_b}\Delta T_\infty e^{i\omega t}. \tag{2.7}$$

The initial condition is taken to be

TABLE 1. Probe and atmospheric properties.

Thermistor bead properties		
k_b	5.36 W m^{-1} K^{-1}	
ρ_b	5331 kg m^{-3}	
c_b	623.7 J kg^{-1} K^{-1}	
α_b	1.612×10^{-6} m^2 s^{-1}	
$R_{b,0}$	20 000 Ω	
$\alpha_{e,b}$	−0.04376 K^{-1}	$\alpha_{e,b} = \frac{1}{R_b}\left.\frac{dR_b}{dT}\right\|_{T=T_0}$
$r_{b,A}$	9.646×10^{-5} m	Bead radius for sphere with same area
$r_{b,v}$	8.936×10^{-5} m	Bead radius for sphere with same volume
Platinum lead-wire properties		
k_w	30 W m^{-1} K^{-1}	
ρ_w	20 500 kg m^{-3}	
c_w	134 J kg^{-1} K^{-1}	
α_w	1.092×10^{-5} m^2 s^{-1}	
$\rho_{e,0}$	1.892×10^{-7} Ω m	
$\alpha_{e,w}$	1.6×10^{-11} K^{-1}	$\alpha_{e,w} = \frac{1}{\rho_{e,0}}\left.\frac{d\rho_{e,0}}{dT}\right\|_{T=T_0}$
r_w	1.0×10^{-5} m	
L	6.385×10^{-4} m	
n	2	Number of wires
Air properties at 300 K and 1 atm		
k_{air}	0.0267 W m^{-1} K^{-1}	
ρ_{air}	1.177 kg m^{-3}	
$c_{p,air}$	1005 J kg^{-1} K^{-1}	
ν_{air}	1.566×10^{-5} m^2 s^{-1}	
Pr_{air}	0.69	
Other conditions		
I	2.5×10^{-5} A	
T_0	300 K	
ΔT_∞	1 K	
V	10 m s^{-1}	

$$T_b(0) = T_0. \quad (2.8)$$

The detailed solution for the bead without wires is given in appendix A. The heat transfer correlation for forced convection over a sphere used to compute the results is given in appendix B.

Equation (A.17) gives the solution to the nondimensional form of Eq. (2.7) subject to the initial condition of Eq. (2.8). However, there is more interest in the periodic term and in finding both the amplitude ratio M_{nw} and the phase shift ϕ_{nw} as functions of frequency. The amplitude ratio is the ratio of the bead temperature amplitude to free-stream air temperature amplitude. The phase shift is due to the time lag between the bead temperature and the free-stream temperature. Using M_{nw} and ϕ_{nw}, the real part of θ_b becomes

$$\mathrm{Re}(\theta_b) = \frac{B_1}{A_1}(1 - e^{-A_1\tau_1}) - \frac{C_1 A_1}{A_1^2 + \omega_1^{*2}} e^{-A_1\tau_1} + M_{nw}\cos(\omega_1^*\tau_1 + \phi_{nw}), \quad (2.9)$$

where

$$M_{nw} = \frac{C_1/A_1}{[1 + (\omega_1^*/A_1)^2]^{1/2}}, \quad (2.10)$$

$$\phi_{nw} = -\arctan\frac{\omega_1^*}{A_1}. \quad (2.11)$$

b. Lumped bead capacity, distributed lead-wire capacity

In this model, as in the previous, the bead temperature is taken to be uniform over its volume but varying in time. The lead wires are assumed to have no gradients in temperature in the radial and azimuthal directions; that is, any cross section perpendicular to the axis of the wire is isothermal (the one-dimensional fin heat transfer approximation). These small Biot number approximations are good for time scales significantly longer than the internal conduction time constants of both the bead and the wire or, equivalently, for frequencies significantly lower than the multiplicative inverse of those time constants.

The transient one-dimensional thermal energy equation for the wire is

$$\rho_w c_w A_{c,w} dx \frac{\partial T}{\partial t} = -k_w A_{c,w}\left(\left.\frac{\partial T}{\partial x}\right|_x - \left.\frac{\partial T}{\partial x}\right|_{x+dx}\right) + h_w P_w dx(T_\infty - T) + \frac{I^2[\rho_{e,0} + \beta_{e,w}(T - T_0)]dx}{A_{c,w}}, \quad (2.12)$$

where ρ_w is the wire mass density, c_w is the wire specific heat, $A_{c,w}$ is the wire cross-sectional area, x is the spatial dimension, T is the wire temperature, k_w is the wire thermal conductivity, h_w is the wire heat transfer coefficient, P_w is the wire circumference, T_∞ is the free-stream temperature, I is the sensing current, $\rho_{e,0}$ is the wire resistivity at T_0, $\beta_{e,w}$ is the wire temperature coefficient of resistivity at T_0, and T_0 is the mean free-stream temperature.

Taking T_∞ as before and simplifying,

$$\frac{\partial T}{\partial t} = \alpha_w \frac{\partial^2 T}{\partial x^2} + \frac{4h_w}{\rho_w c_w d_w}(T_0 + \Delta T_\infty e^{i\omega t} - T) + \frac{16 I^2[\rho_{e,0} + \beta_{e,w}(T - T_0)]}{\pi^2 \rho_w c_w d_w^4}, \quad (2.13)$$

where α_w is the wire thermal diffusivity.

The boundary conditions on the wire are now considered. The thermistor bead is at $x = 0$. The thermal energy equation of the bead is the same as before except there is one more term coupling the bead to the lead wires, and the surface area of the bead is reduced by the wire cross-sectional area times the number of leads, n. The bead has two leads as supplied (see Fig. 1.):

$$m_b c_b \frac{dT_b}{dt} = h_b(A_b - nA_{w,c})(T_0 + \Delta T_\infty e^{i\omega t} - T_b) + I^2[R_{b,0} + \beta_b(T_b - T_0)] + nk_w A_{w,c}\left.\frac{\partial T}{\partial x}\right|_{x=0}. \quad (2.14)$$

The bead temperature T_b is $T(x = 0)$.

The second boundary condition on the wire is at $x = L$, and the two limiting cases previously described are considered:

case (a)

$$T(L, t) = T_0; \quad (2.15)$$

case (b)

$$\left.\frac{\partial T}{\partial x}\right|_{x=L} = 0. \quad (2.16)$$

The detailed solution to Eq. (2.13) subject to the boundary conditions of Eq. (2.14) and either Eq. (2.15) or Eq. (2.16) is given in appendix C. The heat transfer correlations used for obtaining the heat transfer coefficients for the wire and the bead are given in appendix B.

The nondimensional spatial part of the fluctuating component of the bead temperature solution, $\psi(0)$, with the fixed temperature end boundary condition is given by Eq. (C.43), and that with the insulated boundary condition is given by Eq. (C.45). The fluctuating part of the nondimensional temperature of the bead is given as

$$\theta_{b,p} = \psi(0)e^{i\omega^*\tau}, \quad (2.17)$$

and the real part of the fluctuating quantity is

$$\mathrm{Re}(\theta_{b,p}) = \mathrm{Re}[\psi(0)]\cos\omega^*\tau - \mathrm{Im}[\psi(0)]\sin\omega^*\tau. \tag{2.18}$$

Equation (2.18) can also be written in the following form using the amplitude ratio M and phase shift ϕ:

$$\mathrm{Re}(\theta_{b,p}) = M\cos(\omega^*\tau + \phi), \tag{2.19}$$

where

$$M = \langle\{\mathrm{Re}[\psi(0)]\}^2 + \{\mathrm{Im}[\psi(0)]\}^2\rangle^{1/2} \tag{2.20}$$

and

$$\phi = \arctan\frac{\mathrm{Im}[\psi(0)]}{\mathrm{Re}[\psi(0)]}. \tag{2.21}$$

3. Results

Figure 3a shows the transfer function amplitude ratio versus frequency for the ideal bead without lead wires and with two lead wires. The figure shows the response up to 100 Hz because the analysis is valid only for frequencies significantly less than the reciprocal of the internal conduction time constant of the bead, which is about 0.005 s for this case. The two cases for the end conditions of the lead wire are shown: 1) the end insulated, and 2) the end temperature fixed at the mean free-stream temperature. Figure 3a shows that the bead with the wires using the insulated-end boundary condition has an improved response over that of the bead without lead wires for frequencies less than 100 Hz. This result is due to the coupling of the bead and the wire, and the small time constant of the wire. For these conditions, the lead wires act as heat transfer fins that aid the frequency response by improving the thermal coupling between the bead and the air. For frequencies greater than about 0.8 Hz, the response of the bead with wires using the fixed end temperature boundary condition is better than that for the bead without wires, due to the fin effect. For frequencies less than about 0.8 Hz, the response of the bead with the wires with fixed temperature ends is worse than the response of the bead without wires, due to the coupling of the bead to the post temperature. Although it is not easily discernible from the figure, the amplitude ratio of the bead without wires does not go to unity as the frequency goes to zero. This phenomenon is due to the thermistor bead resistance decreasing with temperature, which causes the internal electric heating to decrease as temperature increases and to increase as temperature decreases for constant electric current. Thus, for all frequencies, the response of a material with a resistance that decreases with temperature is worse than one which does not vary with temperature. (Of course if the resistance does not vary with temperature, the material could not be used to measure temperature.) Furthermore, a resistance element that increases with increasing temperature improves the response.

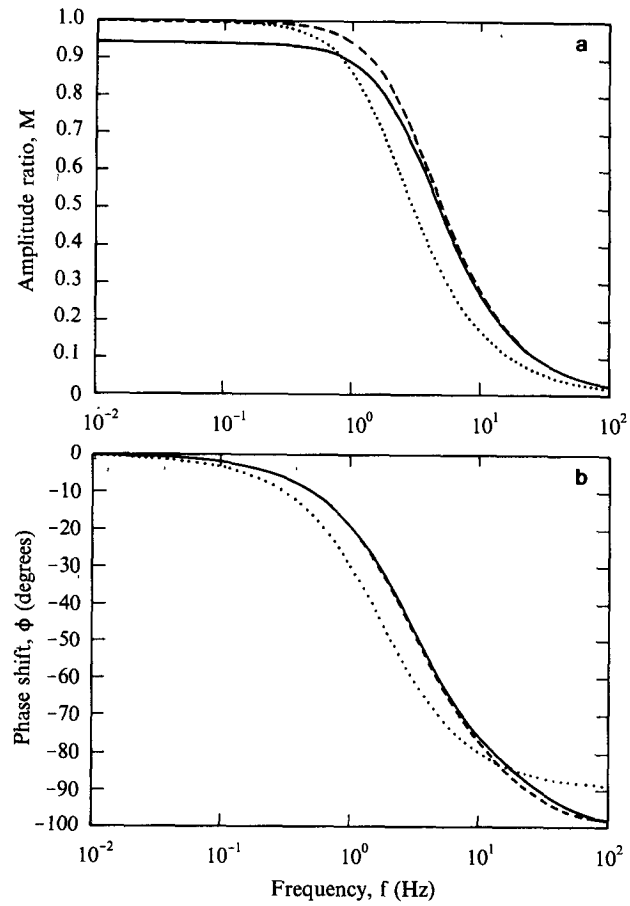

FIG. 3. Transfer function (a) amplitude and (b) phase for two-lead-wire thermistor for $d_w = 20$ μm, $L = 638$ μm lead wire. Dotted line (· · ·) is for no lead wire; solid (——) is for constant temperature support; and dashed (– – –) is for adiabatic support. Frequency f is cyclic frequency (Hz).

Figure 3b shows the phase-shift plot that corresponds to Fig. 3a. For frequencies less than about 20 Hz, the bead with wires does not lag the free-stream temperature as much as the bead without wires. At frequencies greater than 20 Hz, the opposite is true. The wireless bead temperature can lag the free-stream temperature at most by 90°. At higher frequencies the temperature of the bead with wires can lag the free-stream temperature by more than 90° because the bead can lag the wire by at most 90°, and at higher frequencies even the temperature of the small diameter wire lags the free-stream temperature.

As a further illustration of a possible effect on the bead response due to the wire lagging the free stream, Figs. 4a and 4b show the amplitude ratio and phase shift, respectively, for a case the same as in Figs. 3a and 3b, except the wire has a diameter four times larger. The amplitude ratio of the bead with this large wire is worse for very high frequencies. (Of course these frequencies are well above the useful range of the sensor,

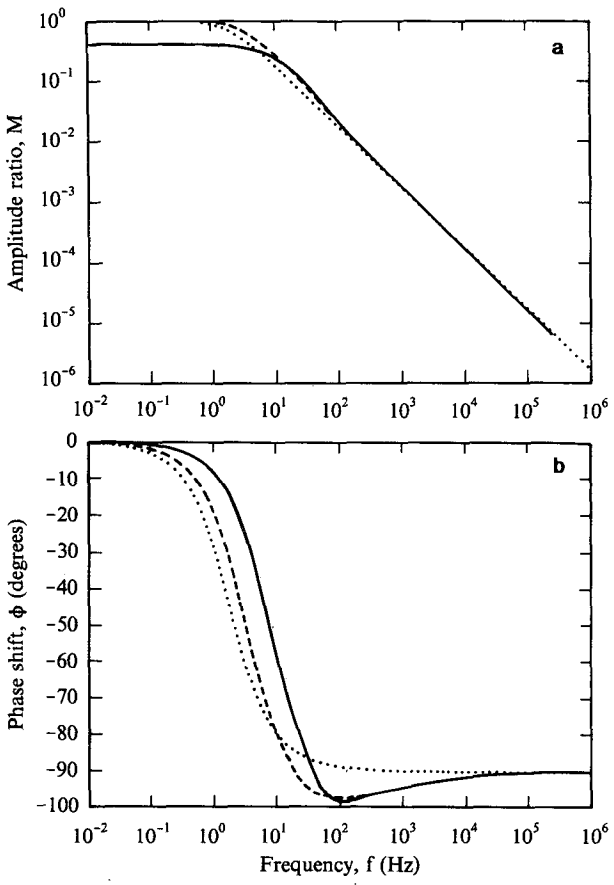

FIG. 4. Expanded transfer function (a) amplitude ratios and (b) phase differences for two-lead-wire thermistor bead, d_w = 80 μm, L = 638 μm, showing crossover of no-lead-wire bead response at approximately 1000 Hz. The line-type representation is the same as in Fig. 3.

but nevertheless still the results demonstrate a possible effect of lead wires that might need consideration in certain situations.) Here it can be seen that the lagging of the wire behind the free-stream temperature not only makes the phase shift worse but also causes the amplitude ratio to be worse than the wireless bead.

Figure 5a shows the effect of wire length on amplitude ratio by displaying the *ratio of the amplitude ratios* of a bead with a given wire length to that of a wireless bead. At low frequencies the bead with the shorter wire is more strongly coupled to the post and therefore has a poorer response. If a given diameter wire is long enough, then the fixed temperature end solution approaches the insulated end solution and there is a negligible end effect. From the dashed curves it is seen that the frequency response of the insulated-end cases for the three longest lengths are virtually identical and independent of length, and the shortest length yields only slightly different results. As for the case shown in Fig. 3, the amplitude ratio M is always less than unity for all frequencies and for any configuration. Figure 5b is the phase-shift plot that corresponds to Fig. 5a and shows the difference between the phase shift of the bead with wires and that without.

Figure 6a shows the effect of wire diameter on amplitude ratio by displaying the ratio of the amplitudes of the bead with wires to that without. The figure shows that there is an optimum value of wire diameter near 40 μm. There are three competing effects to be considered here. As the wire diameter is increased, on the negative side, the wire's response is worse due to a larger thermal mass, and the coupling between the bead and the posts is enhanced. On the positive side, the thermal coupling between the wire and the bead is increased. Figure 6b is the phase-shift difference plot corresponding to Fig. 6a.

The effect of the number of lead wires is shown in Fig. 7a, which is a plot of ratio of amplitude of the bead with lead wires to that without. The plot shows that increasing the number of lead wires improves the response for frequencies greater than 1 Hz. There is a slight reduction in response by increasing the number of wires for frequencies less than 1 Hz, caused by the increased thermal coupling to the posts. Figure 7b

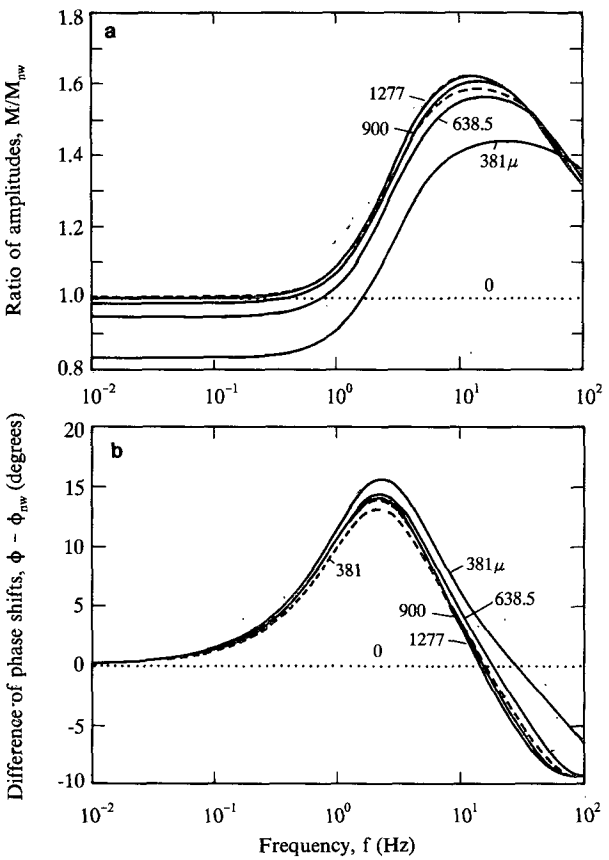

FIG. 5. Frequency response (a) amplitude ratios and (b) phase differences for thermistor bead with two lead wires of lengths L = 381, 638, 900, and 1277 μm relative to L = 0, no-lead-wire case. The line-type representation is the same as in Fig. 3.

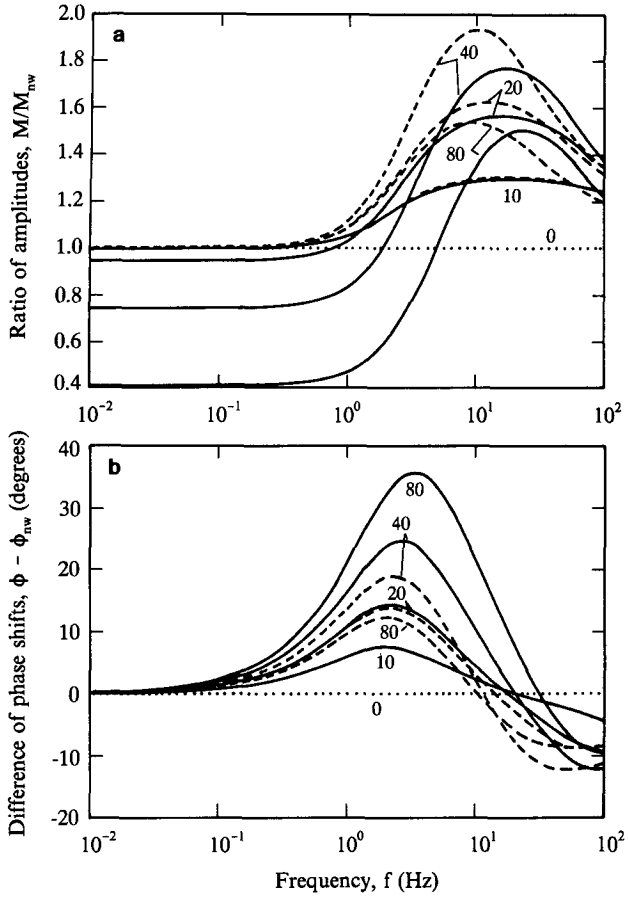

FIG. 6. Frequency response (a) amplitude ratios and (b) phase differences for thermistor bead with two lead wires of L = 638 μm and diameter d_w = 10, 20, 40, and 80 μm relative to d_w = 0, no-lead-wire case. The line-type representation is the same as in Fig. 3.

shows the corresponding phase shift difference plot for Fig. 7a.

Figures 8a and 8b show the results of incorporating the above effects into an improved design. The design was changed from two wires, 638.5 μm long and 20 μm in diameter, to four wires, 1277 μm long and 40 μm in diameter. The solid line is for the fixed-end temperature case, and the dashed line is for the insulated-end case. The ratio of the amplitude of the new design to that of the two-lead-wire case is shown in Fig. 8a. An increase of the magnitude of the transfer function of approximately 67% is seen at about 12 Hz. Figure 8b shows the difference in phase shifts between the two designs. For frequencies less than 12 Hz, the new design has less phase shift than the base case. For frequencies greater than 12 Hz the opposite is true.

One more point worth noting is the offset temperature of the bead due to the internal resistive heating. Normalized by ΔT_∞ the offsets are as follows:

1) for the bead without wires—0.975.

2) for the bead with two wires—20 μm in diameter, and 638.5 μm long, (a) 0.0658 for fixed temperature ends, and (b) 0.0663 for adiabatic ends.

3) for the bead with four wires—40 μm in diameter, and 1275 μm long, (a) 0.0262 for fixed temperature ends, and (b) 0.0263 for adiabatic ends.

The above analysis was also applied to small thermocouple bead sensors, as used by Lawson (1991) and Lawson and Rodi (1992), for example. The details and results are presented in appendix D.

4. Discussion

The analysis and results given herein can be used in the analysis and design of fast-response thermistors and thermocouples for use in atmospheric studies, where good frequency response is necessary for turbulence research. The parameter that can be most easily modified is the wire length, to ensure that thermal coupling to the support posts is minimized. In the manufacturing

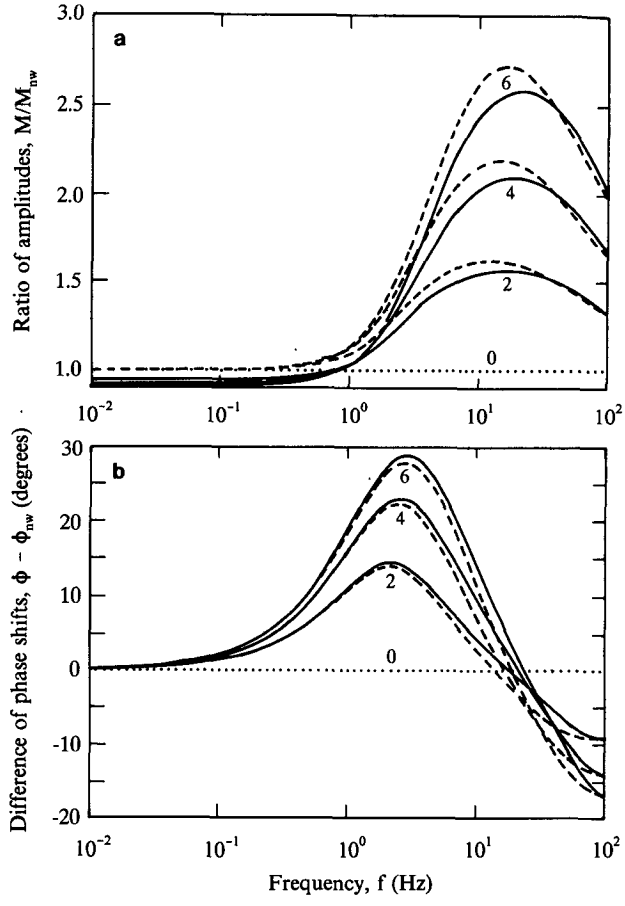

FIG. 7. Frequency response (a) amplitude ratios and (b) phase differences for thermistor bead with lead-wire length L = 638 μm and diameter d_w = 20 μm for 2, 4, and 6 lead wires, relative to n = 0, no-lead-wire case. The line-type representation is the same as in Fig. 3.

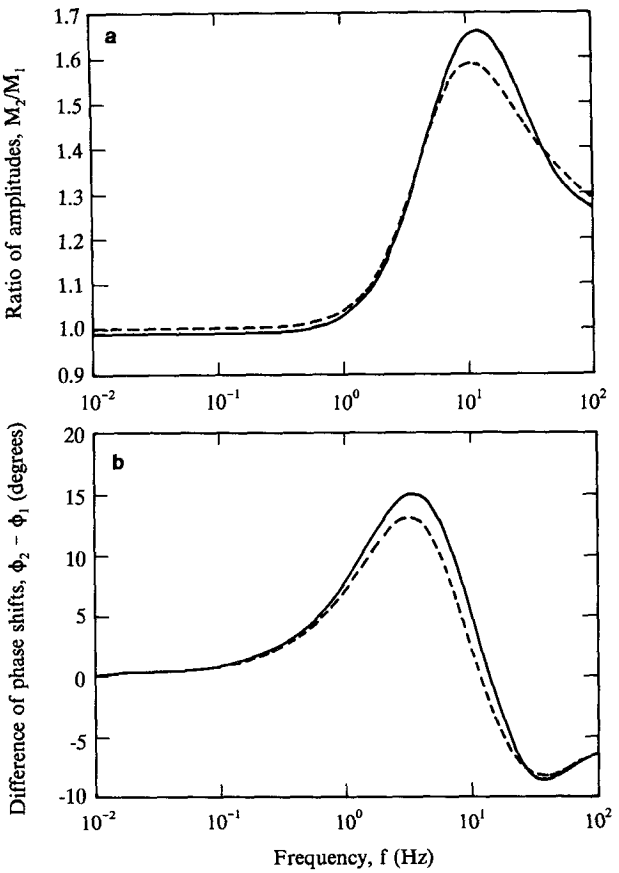

FIG. 8. Frequency response (a) amplitude ratios and (b) phase differences of thermistor bead comparison between 1) base case $n = 2$, $L = 638.5$ μm, and $d_w = 20$ μm and 2) new design $n = 4$, $L = 1277$ μm, $d_w = 40$ μm. The line-type representation is the same as in Fig. 3.

process, the wire diameter, and perhaps for thermistors the number of wires, could be changed. For any given diameter, increasing the lead length to the point where the fixed end temperature response and the insulated end response are almost equal eliminates end effects. By incorporating additional wires, the thermal response is improved through the heat transfer fin effect. The fin effect of the lead wires does mean that a bead-type probe does not follow a simple one-time-constant transfer function for an isolated bead even if support effects are negligible. Sometimes, temperature data are compensated for the response of the probe to obtain higher bandwidth signals [Brum et al. (1983)], and the present work suggests that the lead wire effect should be taken into account.

Structurally, the thermistor assembly also can be improved while improving the thermal frequency response by using multiple wires. Increasing wire diameter requires an increased length for good low-frequency response, a case in which there are competing structural benefits and costs. The addition of wires helps both thermally and structurally.

Acknowledgments. This work was supported by NSF Grant ATM-9024436 and Grant N00014-90-J-1082 from the Office of Naval Research. We would also like to thank Dr. Al Rodi, University of Wyoming, for discussions leading to the inclusion of modeling thermocouples in this study. We would like to thank Minh Tsai for his assistance in the preparation of the manuscript and Sue Fisher for the scanning electron microscope photographs. Finally, we would like to thank an anonymous reviewer for noticing a mistake in the value for the kinematic viscosity of air that made its way into our calculations and that we subsequently corrected.

APPENDIX A

Solution for Bead without Wires

In obtaining a solution it is preferable to consider Eqs. (2.7) and (2.8) in dimensionless form. Nondimensionalizing temperature and time,

$$\theta_b = \frac{(T_b - T_0)}{\Delta T_\infty}, \tag{A.1}$$

$$\tau_1 = \frac{\alpha_b t}{d_{b,v}^2}, \tag{A.2}$$

Eqs. (2.7) and (2.8), respectively, become

$$\frac{d\theta_b}{d\tau_1} = -(6\,\mathrm{Bi}_b d_{b,A/v}^2 - 6L_b)\theta_b + 6K_b + 6\,\mathrm{Bi}_b d_{b,A/v}^2 e^{i\omega_1^* \tau_1}, \tag{A.3}$$

$$\theta_b(0) = 0, \tag{A.4}$$

where

$$\mathrm{Bi}_b = \frac{h_b d_{b,v}}{k_b}, \tag{A.5}$$

$$d_{b,A/v} = \frac{d_{b,A}}{d_{b,v}}, \tag{A.6}$$

$$K_b = \frac{I^2 R_{b,0}}{\pi d_{b,v} k_b \Delta T_\infty}, \tag{A.7}$$

$$L_b = \frac{I^2 \beta_b}{\pi d_{b,v} k_b}, \tag{A.8}$$

$$\omega_1^* = \frac{d_{b,v}^2 \omega}{\alpha_b}. \tag{A.9}$$

The Biot number Bi_b is the ratio of the external heat convection to the internal heat conduction and should be less than 0.1 for the assumption of negligible internal temperature gradients on the bead to hold. The nondimensional parameter K_b is the ratio of mean internal heat generation to conduction. The nondimensional parameter L_b is the ratio of the perturbation of internal heat generation to conduction.

With further rearrangement the nondimensional energy equation becomes

$$\frac{d\theta_b}{d\tau_1} = -A_1\theta_b + B_1 + C_1 e^{i\omega_1^*\tau_1}, \quad \text{(A.10)}$$

where

$$A_1 = (6\ \mathrm{Bi}_b d_{b,A/v}^2 - 6L_b), \quad \text{(A.11)}$$

$$B_1 = 6K_b, \quad \text{(A.12)}$$

and

$$C_1 = 6\ \mathrm{Bi}_b d_{b,A/v}^2. \quad \text{(A.13)}$$

The Laplace transform of Eq. (A.10) is

$$s\Theta_b = -A_1\Theta_b + \frac{B_1}{s} + \frac{C_1}{s - i\omega_1^*}, \quad \text{(A.14)}$$

with the solution

$$\Theta_b = \frac{B_1}{A_1}\left(\frac{1}{s} - \frac{1}{s + A_1}\right) + \frac{C_1}{A_1 + i\omega_1^*}\left(\frac{1}{s - i\omega_1^*} - \frac{1}{s + A_1}\right). \quad \text{(A.15)}$$

The inverse Laplace transform results in the equation

$$\theta_b = \frac{B_1}{A_1}(1 - e^{-A_1\tau_1}) + \frac{C_1(A_1 - i\omega_1^*)}{A_1^2 + \omega_1^{*2}}(e^{i\omega_1^*\tau_1} - e^{-A_1\tau_1}). \quad \text{(A.16)}$$

Taking the real part of θ_b gives

$$\mathrm{Re}(\theta_b) = \frac{B_1}{A_1}(1 - e^{-A_1\tau_1}) - \frac{C_1A_1}{A_1^2 + \omega_1^{*2}}e^{-A_1\tau_1} + \frac{C_1A_1}{A_1^2 - \omega_1^{*2}}(A_1\cos\omega_1^*\tau_1 + \omega_1^*\sin\omega_1^*\tau_1). \quad \text{(A.17)}$$

It is noted that for long times there is a steady-state component equal to B_1/A_1 and a periodic term. The steady-state term is a temperature offset due to the internal $I^2R_{b,0}$ heating; that is, even if the air temperature is constant, the bead will be at slightly higher temperature than the free-stream temperature.

APPENDIX B

Heat Transfer Coefficients for a Sphere and a Cylinder

The heat transfer coefficient h_b is obtained from the Nusselt number Nu_b:

$$h_b = \mathrm{Nu}_b\frac{k_{\mathrm{air}}}{d_{b,v}}, \quad \text{(B.1)}$$

where k_{air} is the air thermal conductivity and $d_{b,v}$ is the equivalent bead diameter for equal volume. The Nusselt number for the bead is a function of Reynolds number and Prandtl number and is given by a correlation for a sphere in the Reynolds number range $0 \leqslant \mathrm{Re} \leqslant 150\,000$ and in the Prandtl number range $\mathrm{Pr} \geqslant 0.6$ (Edwards et al. 1979):

$$\mathrm{Nu}_b = 2 + 0.3\ \mathrm{Re}_b^{0.6}\ \mathrm{Pr}_{\mathrm{air}}^{0.33}, \quad \text{(B.2)}$$

where

$$\mathrm{Re}_b = \frac{Vd_{b,A}}{\nu_{\mathrm{air}}}, \quad \text{(B.3)}$$

and

$$\mathrm{Pr}_{\mathrm{air}} = \frac{\nu_{\mathrm{air}}}{\alpha_{\mathrm{air}}}, \quad \text{(B.4)}$$

where V is the airspeed, ν_{air} is the kinematic viscosity of air, and α_{air} is thermal diffusivity of air.

The wire heat transfer coefficient h_w is obtained from the wire Nusselt number Nu_w,

$$h_w = \mathrm{Nu}_w\frac{k_{\mathrm{air}}}{d_w}, \quad \text{(B.5)}$$

where d_w is the wire diameter. The wire Nusselt number is a function of the wire Reynolds number and the fluid Prandtl number and is given by the correlation of Churchill and Bernstein (1977) for uniform flow over a cylinder where $0 \leqslant \mathrm{Re} < 10\,000$ and $\mathrm{Re\ Pr} > 0.2$:

$$\mathrm{Nu}_w = 0.3 + \frac{0.62\ \mathrm{Re}^{1/2}\ \mathrm{Pr}^{1/3}}{[1 + (0.4/\mathrm{Pr})^{2/3}]^{1/4}}, \quad \text{(B.6)}$$

where

$$\mathrm{Re}_w = \frac{Vd_w}{\nu_{\mathrm{air}}}. \quad \text{(B.7)}$$

APPENDIX C

Solution for Bead with Wires

As in the case for the bead without wires, a dimensionless solution to Eq. (2.13) subject to boundary conditions of Eq. (2.14) and either Eq. (2.15) or Eq. (2.16) is preferable. Nondimensionalizing temperature T, time t, and spatial coordinate x gives

$$\theta = \frac{T - T_0}{\Delta T_\infty}, \quad \text{(C.1)}$$

$$\tau = \frac{\alpha_w t}{d_w^2}, \quad \text{(C.2)}$$

$$\eta = \frac{x}{d_w}. \quad \text{(C.3)}$$

The nondimensional wire energy equation is thus

$$\frac{\partial\theta}{\partial\tau} = \frac{\partial^2\theta}{\partial\eta^2} - 4(\mathrm{Bi}_w - 4L_w)\theta + 16K_w + 4\,\mathrm{Bi}_w e^{i\omega^*\tau}, \tag{C.4}$$

where

$$\mathrm{Bi}_w = \frac{h_w d_w}{k_w}, \tag{C.5}$$

$$K_w = \frac{I^2\rho_{e,0}}{\pi^2 d_w^2 k_w \Delta T_\infty}, \tag{C.6}$$

$$L_w = \frac{I^2\beta_w}{\pi^2 d_w^2 k_w}, \tag{C.7}$$

$$\omega^* = \frac{d_w^2\omega}{\alpha_w}. \tag{C.8}$$

The nondimensional parameters Bi_w, K_w, and L_w, for the wire have the same physical meaning as their counterparts for the bead. Simplifying notation further, the nondimensional energy equation becomes

$$\frac{\partial\theta}{\partial\tau} = \frac{\partial^2\theta}{\partial\eta^2} - A\theta + B + Ce^{i\omega^*\tau}, \tag{C.9}$$

where

$$A = 4(\mathrm{Bi}_w - 4L_w), \tag{C.10}$$

$$B = 16K_w, \tag{C.11}$$

$$C = 4\,\mathrm{Bi}_w. \tag{C.12}$$

Nondimensionalizing the bead energy equation in the same manner as for the wire, simplifying, and rearranging gives

$$\left.\frac{\partial\theta}{\partial\eta}\right|_{\eta=0} = \frac{2}{3nk_r d_r\tau_r}\frac{d\theta_b}{d\tau} + \frac{3\,\mathrm{Bi}_b(d_{b,A/v}^2 - nd_r^2) - 2L_b}{3nk_r d_r}\theta_b - \frac{2K_b}{3nk_r d_r} - \frac{\mathrm{Bi}_b(d_{b,A/v}^2 - nd_r^2)}{nk_r d_r}e^{i\omega^*\tau}. \tag{C.13}$$

The nondimensional bead energy equation gives one boundary condition on the nondimensional temperature at $\eta = 0$. The nondimensional parameters Bi_b, K_b, L_b, and $d_{b,A/v}$ are the same as in the case of the bead without lead wires, and

$$k_r = \frac{k_w}{k_b}, \tag{C.14}$$

$$d_r = \frac{d_w}{d_{b,v}}, \tag{C.15}$$

$$\tau_r = \frac{\tau_w}{\tau_b} = \frac{d_w^2/\alpha_w}{d_{b,v}^2/\alpha_b}. \tag{C.16}$$

After simplifying the notation, the bead energy equation/wire boundary condition becomes

$$\left.\frac{\partial\theta}{\partial\eta}\right|_{\eta=0} = D\frac{d\theta_b}{d\tau} + E\theta_b - F - Ge^{i\omega^*\tau}, \tag{C.17}$$

where

$$D = \frac{2}{3nk_r d_r\tau_r}, \tag{C.18}$$

$$E = \frac{3\,\mathrm{Bi}_b(d_{b,A/v}^2 - nd_r^2) - 2L_b}{3nk_r d_r}, \tag{C.19}$$

$$F = \frac{2K_b}{3nk_r d_r}, \tag{C.20}$$

$$G = \frac{\mathrm{Bi}_b(d_{b,A/v}^2 - nd_r^2)}{nk_r d_r}. \tag{C.21}$$

The boundary condition at the post, $x = L$, for each case is also given in nondimensional form as

case (a),

$$\theta(\eta = L^*) = 0, \tag{C.22}$$

case (b),

$$\left.\frac{\partial\theta}{\partial\eta}\right|_{\eta=L^*} = 0, \tag{C.23}$$

where $L^* = L/d_w$.

Equation (C.9) is solved subject to the boundary conditions of Eq. (C.17) and either Eq. (C.22) or Eq. (C.23). The solution sought is the steady periodic solution, which requires no initial condition, because the solution is at times long enough such that all initial transients have become negligible. The solution has the form of a spatially dependent steady term added to a spatially dependent fluctuating term; namely,

$$\theta(\eta, \tau) = \bar{\theta}(\eta) + \psi(\eta)e^{i\omega^*\tau}. \tag{C.24}$$

The nondimensional bead temperature is thus given by

$$\theta_b(\tau) = \theta(0, \tau) = \bar{\theta}(0) + \psi(0)e^{i\omega^*\tau}. \tag{C.25}$$

Substituting for θ from Eq. (C.24) into Eqs. (C.9), (C.17), (C.22), and (C.23) gives

$$i\omega^*\psi e^{i\omega^*\tau} = \frac{d^2\bar{\theta}}{d\eta^2} + \frac{d^2\psi}{d\eta^2}e^{i\omega^*\tau} - A\bar{\theta} - A\psi e^{i\omega^*\tau} + B + Ce^{i\omega^*\tau}, \tag{C.26}$$

with the boundary conditions

$$\left.\frac{d\bar{\theta}}{d\eta}\right|_{\eta=0} + \left.\frac{d\psi}{d\eta}\right|_{\eta=0}e^{i\omega^*\tau} = Di\omega^*\psi(0)e^{i\omega^*\tau} + E\bar{\theta}(0) + E\psi(0)e^{i\omega^*\tau} - F - Ge^{i\omega^*\tau}; \tag{C.27}$$

case (a):

$$\bar{\theta}(L^*) + \psi(L^*)e^{i\omega^*\tau} = 0; \qquad \text{(C.28)}$$

case (b):

$$\left.\frac{d\bar{\theta}}{d\eta}\right|_{\eta=L^*} + \left.\frac{d\psi}{d\eta}\right|_{\eta=L^*} e^{i\omega^*\tau} = 0. \qquad \text{(C.29)}$$

Time averaging Eqs. (C.26)–(C.29) over one period ($2\pi/\omega^*$) yields

$$\frac{d^2\bar{\theta}}{d\eta^2} = A\bar{\theta} - B, \qquad \text{(C.30)}$$

with the boundary conditions

$$\left.\frac{d\bar{\theta}}{d\eta}\right|_{\eta=0} = E\bar{\theta}(0) - F; \qquad \text{(C.31)}$$

case (a):

$$\bar{\theta}(L^*) = 0; \qquad \text{(C.32)}$$

case (b):

$$\left.\frac{d\bar{\theta}}{d\eta}\right|_{\eta=L^*} = 0. \qquad \text{(C.33)}$$

Equation (C.30) is the mean nondimensional governing differential equation, Eq. (C.31) is the boundary condition on the mean nondimensional temperature at the bead, and Eqs. (C.32) and (C.33) are the two different boundary conditions at the posts.

Solving Eq. (C.30) with boundary conditions Eq. (C.31) and case (a), Eq. (C.32), or case (b), Eq. (C.33) gives the solution for the mean nondimensional temperature distribution in the wire with case (a) the support-post end temperature at the mean free-stream value, or case (b) the support-post end insulated. Furthermore, evaluating $\bar{\theta}$ at $\eta = 0$ gives the mean nondimensional temperature offset due to internal heating and lead effects.

The solution for case (a) is

$$\bar{\theta}(\eta) = \frac{B}{A} - \frac{(EB - FA)\sinh[A^{1/2}(L^* - \eta)] + B[A^{1/2}\cosh(A^{1/2}\eta) + E\sinh(A^{1/2}\eta)]}{A[A^{1/2}\cosh(A^{1/2}L^*) + E\sinh(A^{1/2}L^*)]}, \qquad \text{(C.34)}$$

and

$$\bar{\theta}(0) = \frac{B}{A} - \frac{(EB - FA)\sinh(A^{1/2}L^*) + BA^{1/2}}{A[A^{1/2}\cosh(A^{1/2}L^*) + E\sinh(A^{1/2}L^*)]}. \qquad \text{(C.35)}$$

The solution for case (b) is

$$\bar{\theta}(\eta) = \frac{B}{A} - \frac{(EB - FA)\cosh[A^{1/2}(L^* - \eta)]}{A[A^{1/2}\sinh(A^{1/2}L^*) + E\cosh(A^{1/2}L^*)]}, \qquad \text{(C.36)}$$

and

$$\bar{\theta}(0) = \frac{B}{A} - \frac{(EB - FA)\cosh(A^{1/2}L^*) + BA^{1/2}}{A[A^{1/2}\cosh(A^{1/2}L^*) + E\sinh(A^{1/2}L^*)]}. \qquad \text{(C.37)}$$

Next, the periodic components are examined. Subtracting the time-averaged equations, Eqs. (C.30)–(C.33), from the full time-dependent equations, Eqs. (C.26)–(C.29), respectively, and simplifying gives the equations governing the periodic components

$$\frac{d^2\psi}{d\eta^2} = (A + i\omega^*)\psi - C, \qquad \text{(C.38)}$$

with the boundary conditions

$$\left.\frac{d\psi}{d\eta}\right|_{\eta=0} = (Di\omega^* + E)\psi(0) - G; \qquad \text{(C.39)}$$

case (a):

$$\psi(L^*) = 0; \qquad \text{(C.40)}$$

case (b):

$$\left.\frac{d\psi}{d\eta}\right|_{\eta=L^*} = 0. \qquad \text{(C.41)}$$

The solution for case (a) is

$$\psi(\eta) = \frac{C}{A + i\omega}\left\{1 - \frac{\cosh[(A + i\omega^*)^{1/2}\eta]}{\cosh[(A + i\omega^*)^{1/2}L^*]}\right\} + \frac{[(G(A + i\omega^*) - C(Di\omega^* + E))\cosh[(A + i\omega^*)^{1/2}L^*] + C(Di\omega^* + E)]\sinh[(A + i\omega^*)^{1/2}(L^* - \eta)]}{(A + i\omega^*)\cosh[(A + i\omega^*)^{1/2}L^*] \times \{(A + i\omega^*)^{1/2}\cosh[(A + i\omega^*)^{1/2}L^*] + (Di\omega^* + E)\sinh[(A + i\omega^*)^{1/2}L^*]\}}, \qquad \text{(C.42)}$$

and

$$\psi(0) = \frac{C\{\cosh[(A + i\omega^*)^{1/2}L^*] - 1\} + G(A + i\omega^*)^{1/2}\sinh[(A + i\omega^*)^{1/2}L^*]}{(A + i\omega^*)^{1/2}\{(A + i\omega^*)^{1/2}\cosh[(A + i\omega^*)^{1/2}L^*] + (Di\omega^* + E)\sinh[(A + i\omega^*)^{1/2}L^*]\}}. \quad \text{(C.43)}$$

The solution for case (b) is

$$\psi(\eta) = \frac{C}{A + i\omega^*} + \frac{[G(A + i\omega^*) - C(Di\omega^* + E)]\cosh[(A + i\omega^*)^{1/2}(L^* - \eta)]}{(A + i\omega^*)\{(A + i\omega^*)^{1/2}\sinh[(A + i\omega^*)^{1/2}L^*] + (Di\omega^* + E)\cosh[(A + i\omega^*)^{1/2}L^*]\}}, \quad \text{(C.44)}$$

and

$$\psi(0) = \frac{C\sinh[(A + i\omega^*)^{1/2}L^*] + G(A + i\omega^*)^{1/2}\cosh[(A + i\omega^*)^{1/2}L^*]}{(A + i\omega^*)^{1/2}\{(A + i\omega^*)^{1/2}\sinh[(A + i\omega^*)^{1/2}L^*] + (Di\omega^* + E)\cosh[(A + i\omega^*)^{1/2}L^*]\}}. \quad \text{(C.45)}$$

APPENDIX D

Thermocouple Response

The above model was applied to the sizes of thermocouples used by Lawson and Rodi (1992) for an in-cloud aircraft temperature probe; 12.5-, 25-, and 50-μm wire diameter with 1-mm leads. Figure D1 shows electron microscope photographs of the 12.5- and 25-μm thermocouples. The thermocouple junctions were modeled as spheres with three times the diameter of the wires, based on the photographs, and the thermal properties of the spheres were taken to be the average of the two thermocouple materials (chromel and constantan for type-E thermocouples). In the actual probe, each lead wire is a different metal; the model was run twice with both wires identical, once with chromel properties and once with constantan properties. In the model of the thermocouple, no I^2R heating is considered, and the airspeed was taken to be 70 m s^{-1} because the thermocouples were flown in the free stream with no housing in the Lawson and Rodi (1992) probe.

The amplitude ratio and phase-shift plots are shown in Fig. D2 for chromel lead wires. (Since the thermal properties of the materials are not very different, the response curves are very similar for constantan and thus are not shown.) This result allows the preceding analysis to be used with the assumption of either wire's thermal properties, or some mean values. Also, the wires are long enough that the fixed temperature end results and the insulated end results are virtually identical for the 12.5- and 25-μm wires. For the length of 1 mm considered here, there is no major end effect since the 70 m s^{-1} airspeed gives a high heat transfer coefficient and thermocouple alloys are poor thermal conductors. Of course the response is improved with decreasing thermocouple diameter. Like the thermistor probe, the thermocouple wires on either side of the junction also act as heat transfer fins and improve the frequency response.

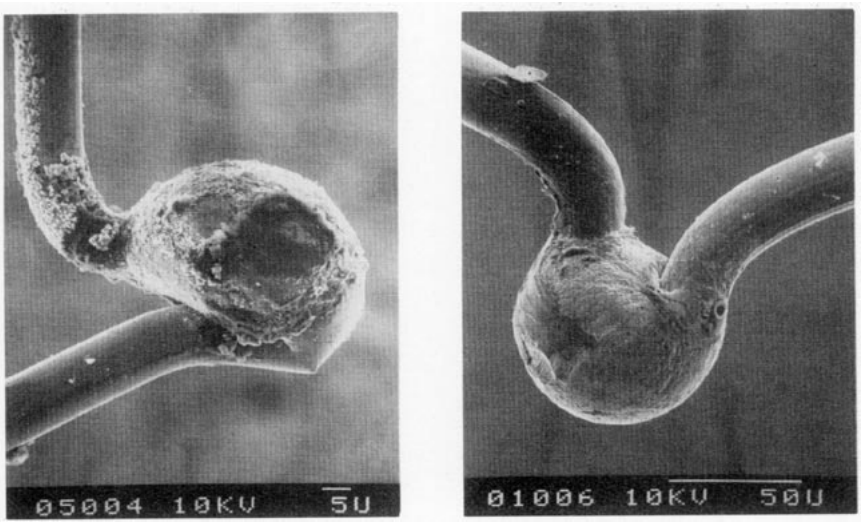

FIG. D1. Scanning electron microscope photograph of a typical thermocouple junction of 12.5-μm and 25-μm wires (Model CHCO-0005 Omega Engineering Co., Stanford, Connecticut).

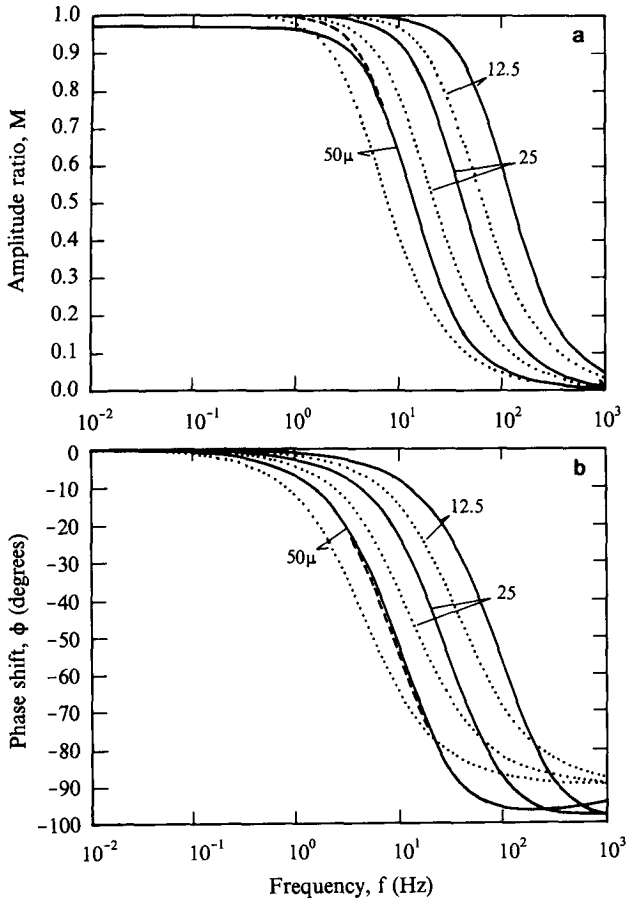

FIG. D2. Transfer function (a) amplitude and (b) phase for chromel lead wire $L = 0$ and 1.0 mm (1000 μm) and diameter $d_w = 12.5$, 25, and 50 μm.

REFERENCES

Brum, R. D., E. T. Seiler, J. C. LaRue, and G. S. Samuelsen, 1983: Instantaneous two-component laser anemometry and temperature measurements in a complex flow model combustor. *21st Aerospace Sciences Meeting,* Reno, Amer. Inst. Aero. and Astro., 9 pp.

Cheney, N. R., and J. A. Businger, 1990: An accurate fast response temperature system using thermocouples. *J. Atmos. Oceanic Technol.,* **7,** 504–516.

Churchill, S. W., and M. Bernstein, 1977: A correlating equation for forced convection from gases and liquids to a circular cylinder in crossflow. *J. Heat Transfer, Trans. ASME,* **94,** 300–306.

Edwards, D. K., V. E. Denny, and A. F. Mills, 1979: *Transfer Processes.* McGraw-Hill, 421 pp.

Friehe, C. A., and D. Khelif, 1993: Fast-response aircraft temperature sensors. *J. Atmos. Oceanic Technol.,* **9,** 784–795.

Lawson, R. P., 1991: Design and preliminary tests of a new airborne thermometer. *Seventh Symp. on Meteorological Observations and Instrumentation,* New Orleans, Amer. Meteor. Soc., 366–371.

——, and A. R. Rodi, 1992: A new airborne thermometer for atmospheric and cloud physics research. Part I: Design and preliminary flight tests. *J. Atmos. Oceanic Technol.,* **9,** 556–574.

Lumley, J. L., 1962: The constant temperature hot-thermistor anemometer. *Symp. on Measurement in Unsteady Flow,* New York, The American Society of Mechanical Engineers.

Paranthoen, P., C. Petit, and J. C. Lecordier, 1982: The effect of the thermal prong-wire interaction on the response of a cold wire in gaseous flows (air, argon, and helium). *J. Fluid Mech.,* **124,** 457–473.

Payne, G. A., C. A. Friehe, and D. K. Edwards, 1994: Time and frequency response of a resistance-wire aircraft atmospheric temperature sensor. *J. Atmos. Oceanic Technol.,* **11,** 463–475.

Samsonov, G. V., Ed., 1982: *The Oxide Handbook.* 2d ed. IFI Plenum, 463 pp.

Sandborn, V. A., 1972: *Resistance Temperature Transducers.* Metrology Press, 545 pp.

Thermometrics, 1987: *Thermistor Sensor Handbook.* Thermometrics, Inc., 199 pp.